How to cite: *Angew. Chem. Int. Ed.* **2020**, *59*, 13785–13792
International Edition: doi.org/10.1002/anie.202005730
German Edition: doi.org/10.1002/ange.202005730

2D Materials

Site-Selective Oxidation of Monolayered Liquid-Exfoliated WS_2 by Shielding the Basal Plane through Adsorption of a Facial Amphiphile

*Sebastian Grieger, Beata M. Szydłowska, Vaishnavi J. Rao, Eva Steinmann, Marcus Dodds, Zahra Gholamvand, Georg S. Duesberg, Jana Zaumseil, and Claudia Backes**

Abstract: *In recent years, various functionalization strategies for transition-metal dichalcogenides have been explored to tailor the properties of materials and to provide anchor points for the fabrication of hybrid structures. Herein, new insights into the role of the surfactant in functionalization reactions are described. Using the spontaneous reaction of WS_2 with chloroauric acid as a model reaction, the regioselective formation of gold nanoparticles on WS_2 is shown to be heavily dependent on the surfactant employed. A simple model is developed to explain the role of the chosen surfactant in this heterogeneous functionalization reaction. The surfactant coverage is identified as the crucial element that governs the dominant reaction pathway and therefore can severely alter the reaction outcome. This study shows the general importance of the surfactant choice and how detrimental or beneficial a certain surfactant can be to the desired functionalization.*

Introduction

Van-der-Waals crystals are a promising class of nanomaterials owing to the exotic properties originating from their layered structure.[1] Popular representatives are the transition-metal dichalcogenides (TMDs). The group of TMDs consists of MX_2 compounds in which M denotes a transition metal in the oxidation state +IV and X are chalcogen atoms, such as S, Se, or Te.[2] To access the promised remarkable properties of two-dimensional nanomaterials, significant effort has been directed towards efficient means of exfoliation and functionalization. One increasingly popular top-down technique to produce nanosheets is liquid-phase exfoliation (LPE), which results in colloidally stable dispersions with widely pristine properties of the nanosheets.[3] Here the interlayer forces are usually overcome by sonication of layered, crystalline bulk materials. Reaggregation of the exfoliated material can be readily suppressed by working in a suitable solvent or surfactant solution of choice, most commonly aqueous sodium cholate (SC) or sodium dodecyl sulfate (SDS) solution.[4] The produced nanomaterial dispersions are intrinsically polydisperse in lateral size and layer number of the nanosheets, but post-exfoliation size selection can be achieved via centrifugation.[5]

Chemical functionalization of nanomaterials has attracted attention to further tailor the already promising traits of nanomaterials.[6] Even though widely considered chemically inert, a range of functionalization strategies for TMDs have been reported in the last decade.[6a,d] Common practices to facilitate functionalization exploit activation of the sheets by reductive chemical exfoliation (CE). Here, the TMDs are partially or completely reduced using alkyl lithium reducing agents and subsequently transformed into their metallic 1T-polytype (such as in the case of MoS_2 or WS_2).[2] Owing to charge being present, colloidally stable dispersions are obtained, but the nanosheets are rather defective. As such, CE-TMDs are more easily functionalized than pristine, semiconducting TMDs in their 2H-polytype for example in electrophilic addition reactions[7] or functionalization at defect sites.[8] A few recent reports also show strategies for the functionalization of the 2H-polytype, for example, coordination of the chalcogen to metal ions,[9] electrophilic addition with diazonium salts,[10] Michael addition of the TMD sulfur with maleimides,[11] or coordination of dithiolane derivatives or thionine to specific undercoordinated edge sites.[12]

Dispersions of nanomaterials are particularly suitable for functionalization owing to the efficiency and versatility of wet chemical methods, yet the reaction mechanisms for these heterogeneous reactions leading to functionalization are often not well understood. For example, a surprising regioselectivity was found in the recently reported spontaneous redox reaction of LPE WS_2 with chloroauric acid, which resulted in the formation of covalently bound nanoparticles to edges of the nanosheets.[13] By controlling the reaction

[*] S. Grieger, B. M. Szydłowska, V. J. Rao, E. Steinmann, M. Dodds, J. Zaumseil, C. Backes
Institute for Physical Chemistry
Ruprecht-Karls-Universität Heidelberg
Im Neuenheimer Feld 253, 69120 Heidelberg (Germany)
E-mail: backes@uni-heidelberg.de
B. M. Szydłowska, G. S. Duesberg
Institute of Physics, EIT 2, Faculty of Electrical Engineering and Information Technology, Universität der Bundeswehr München
Werner-Heisenberg-Weg 39, 85577 Neubiberg (Germany)
Z. Gholamvand
School of Physics and CRANN & AMBER Research Centres
Trinity College Dublin, Dublin 2 (Ireland)
J. Zaumseil
Centre for Advanced Materials
Ruprecht-Karls-Universität Heidelberg
Im Neuenheimer Feld 225, 69120 Heidelberg (Germany)
Supporting information and the ORCID identification number(s) for the author(s) of this article can be found under: https://doi.org/10.1002/anie.202005730.

conditions, it was possible to remove heavy mass aggregates of Au@WS_2 to isolate predominantly monolayers in high yield with small (2–4 nm) Au nanoparticles at edges. It was proposed that the chloroauric acid reacts with the thiol groups at the nanosheet edges forming the nucleation centers that lead to edge decoration.[13] However, the exact mechanism responsible for the observed regioselective decoration, as well as the monolayer enrichment has not been understood. In particular, the role that the surfactant stabilizer plays in the reaction has not been investigated.

Ionic surfactants are widely used in stabilizing colloidal nanomaterials such as carbon nanotubes,[14] graphene,[15] h-BN,[16] or TMDs.[17] Generally, they can be roughly divided into facial and linear amphiphiles. Commonly used facial amphiphiles are various representatives of the bile salt family, such as SC.[18] Generally, their structure can be divided into a bulky, sterane-like body of highly rigid annulated cycloalkanes, with polar substituents (mostly hydroxide groups) on one face of the body and hydrophobic substituents on the opposing face.[19] In contrast, linear amphiphiles such as SDS adhere to the structural head-tail motif with a hydrophilic head group and long, hydrophobic alkyl chains. Owing to their different chemical structures, facial and linear amphiphiles behave differently. For example, linear amphiphiles adsorb as hemicylindrical micelles with the alkyl chains lying flat on the surface in random orientation and polar head groups bending towards the surrounding solution resulting in rapid exchange of free and bound surfactants.[20] However, for facial amphiphiles such as SC, where hydrogen bonding is possible,[21] the hydrophobic side of the body is expected to face the nanomaterial surface, whereas the hydrophilic side points towards the solution, and side-to-side aggregation is expected to minimize the exposure of the hydrophobic face to water.[19] Therefore, a certain impact of the choice of surfactant on functionalization reactions can be expected and has been proposed beforehand for graphene.[19] However, no reported studies exist to undermine this. This is attributed to the difficulty in the characterization of potentially regioselective functionalized materials (for example, edge versus basal plane).

Herein we address these points. In particular, we present a case study that shows that the choice of surfactant can have a significant impact on the reactivity of LPE TMDs. We arrive at new insights into the Au nanoparticle decoration reaction and propose a simple model for the spontaneous formation of defined gold nanoparticles upon oxidation of WS_2 with chloroauric acid. This reaction was chosen owing to the distinct absorption signals of chloroauric acid and gold nanoparticles, as well as the good contrast of gold in transmission electron microscopy, which facilitates characterization of the system and therefore enables detailed analysis of this heterogeneous reaction, unlike functionalization with discrete molecular species. We believe the reaction serves as a general case study for the influence and role of the surfactant in functionalization reactions using molecular reagents.

Results and Discussion

To test the impact of the surfactant coverage on the reactivity of LPE WS_2, we chose the previously reported[13] reaction with chloroauric acid as a model reaction. It has been shown that WS_2 nanosheets in colloidal dispersion obtained from sonication-assisted LPE undergo a spontaneous redox reaction with chloroauric acid. This results in a dispersion of red color, which after work-up and purification yields monolayer-rich, selectively edge-decorated WS_2 nanosheet gold nanoparticle composites (Au@WS_2).[13] It was demonstrated that size and density of the nanoparticles can be tuned by the stoichiometry ratio of chloroauric acid and WS_2. The reaction is useful, as it is a facile approach to isolate WS_2 monolayers of various sizes with optical properties (such as narrow linewidth photoluminescence) retained.[13] In the following, we will describe a series of experiments using two different surfactant stabilizers to shine light on the reaction mechanism and gain a deeper understanding of the oxidation of WS_2 nanosheets in surfactant stabilized dispersions.

As surfactants, we chose the facial amphiphile sodium cholate (SC, Figure 1 A) and the linear amphiphile sodium dodecyl sulfate (SDS, Figure 1 B). In both cases, WS_2 powder was immersed in the respective aqueous surfactant solution (23 mM) and subjected to tip sonication. Unexfoliated WS_2 and very small nanosheets were then removed by centrifugation (see the Supporting Information, Methods). No further size selection was performed prior to reaction with chloroauric acid. As such, the WS_2 samples are polydisperse in size with a broad distribution of lateral dimensions ranging from 50–400 nm and thicknesses from 1–40 layers.[17] In such samples, monolayer contents are very low ($< 0.5\,\%$).[17] The concentration of WS_2 in dispersion was adjusted to $0.5\,g\,L^{-1}$ prior to mixing with an aqueous solution of chloroauric acid 1:1 by volume. The molar stoichiometry ratio of chloroauric acid to WS_2 was initially fixed to 4 equiv, as this was previously identified as ideal ratio of the reagents to achieve efficient isolation of edge-decorated monolayers.[13] Chloroauric acid was added dropwise under cooling (see the Supporting Information, Methods). For both SC and SDS, a spontaneous reaction is observed as evident by a color change from yellowish-green (owing to WS_2) to dark red–purple in SC and blue–black in SDS (characteristic of Au nanoparticles and their aggregates, respectively).[22] Unreacted chloroauric acid was removed in the supernatant after centrifugation at high centrifugal accelerations (expressed as relative centrifugal force, RCF, in units of the earth's gravitational field, g) and large, heavy mass aggregates as sediment after centrifugation at low centrifugal accelerations (Figure 1 C; Supporting Information, Methods). The sediment after this low speed centrifugation is denoted as work-up sediment, while the supernatant is denoted as stock.

Transmission electron microscopy (TEM) was performed on various samples extracted from the respective stock dispersions using iterative centrifugation with subsequently increasing centrifugal acceleration, which is called purification hereafter (Figure 1 D; Supporting Information, Methods). In general, such a procedure results in a size selection predominantly by material mass/density[18b,23] and it was used

in the previous study to enrich the dispersion in WS_2 monolayers decorated with small gold nanoparticles (2–4 nm diameter) at the edges.[13,24] Representative images are shown in Figure 1 E–H (more images, see the Supporting Information, Figure S1). Au nanoparticles with intense contrast are seen in all cases. In the purification sediment extracted at high RCF, almost exclusively edge-decorated nanosheets are observed with SC as surfactant (Figure 1 E), in accordance with previous reports.[13,24] In contrast, with SDS as surfactant, almost exclusively free gold nanoparticles and no nanosheets with characteristic shape are observed (Figure 1 F). In the case of the purification sediment extracted at low RCF, that is, the first centrifugation step in the purification, relatively large but well-defined gold nanoparticles are formed on top of edge-decorated nanosheets in SC (Figure 1 G), which is possibly due to basal plane nucleation, whereas in the case of SDS we find big, ill-defined gold structures as well as non-edge decorated nanosheets that appear less electron transparent and therefore few-layered (Figure 1 H). In this sample, nanosheets are a minority fraction and the edges of the nanosheets appear disrupted hinting towards degradation/oxidation. This suggests that the reaction takes a different pathway depending on the surfactant.

To elaborate this difference between SC and SDS as surfactant further, we conducted optical extinction spectroscopy on samples extracted during purification from the polydisperse stock Au-WS_2 dispersion (Figure 1 D). As shown by the extinction spectra in Figure 2 A, the pristine optical properties of WS_2 are retained with SC as surfactant in the material isolated at high RCF on purification (orange trace), where heavily Au decorated nanosheets are removed in agreement with previous observations.[13] The removal of Au-rich material at low and intermediate RCF results in a reduction of the relative contribution of the Au surface plasmon resonance at 450–650 nm to the optical extinction so that the characteristic excitonic transitions of WS_2[25] dominate the spectra. This agrees well with the removal of big gold nanoparticles observed in TEM imaging (Figure 1 E,G). However, when performing the reaction in SDS, a generally different behavior can be observed. The dispersion turns initially blue–black and does not recover the original color of pristine WS_2 in the different fractions of the purification cascade. This is reflected in the spectral shape of the extinction spectra for the purified material (Figure 2 B) which show a broad absorbance at >450 nm due to the presence of large, ill-defined Au structures (as evidenced from TEM, Figure 1 H). Even in the material isolated at high RCF, the excitonic transitions of the WS_2 are not clearly resolved.

This strongly suggests an involvement of the surfactant in the decoration reaction. SC as well as SDS alone do not react with chloroauric acid under the experimental conditions

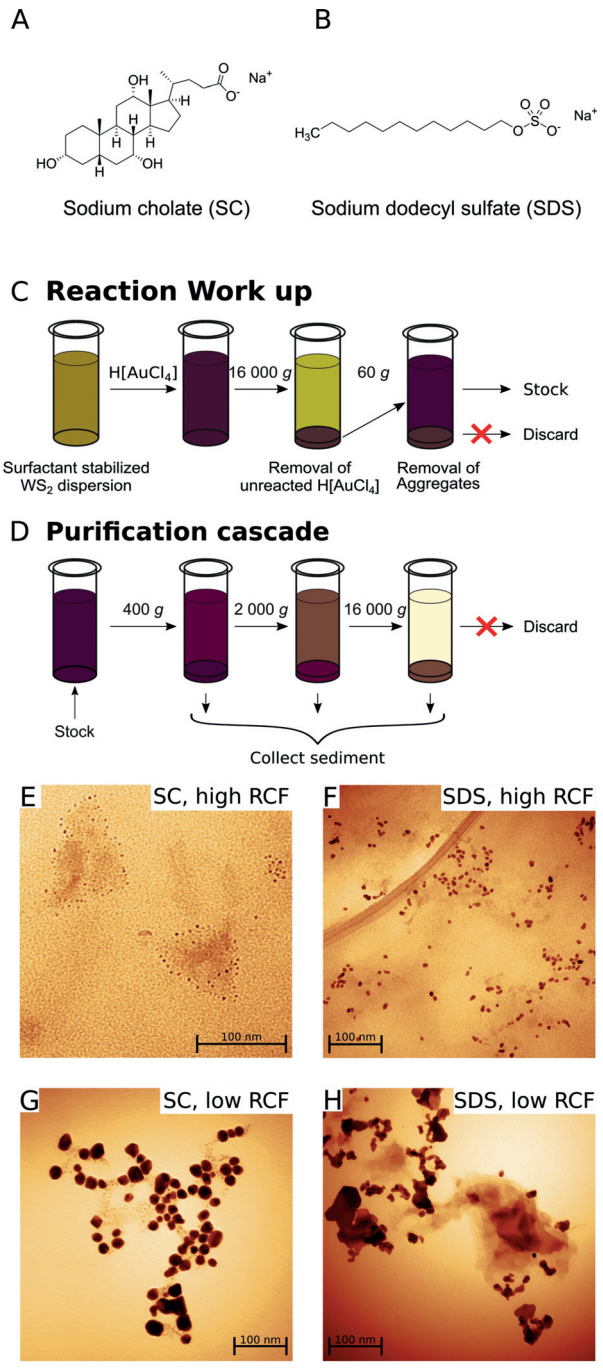

Figure 1. A),B) Structural formulas of the surfactants used in this study: A) Sodium cholate (SC) and B) sodium dodecyl sulfate (SDS). C) The work-up after reaction of LPE WS_2 with chloroauric acid. At high centrifugal acceleration (16 000 g), unreacted chloroauric acid is removed in the supernatant, while heavy mass aggregates are removed as sediment at low centrifugal acceleration (60 g) and typically discarded. D) The centrifugation cascade for further purification previously used to isolate WS_2 monolayers with minimal Au^0 content. E)–H) TEM images (120 kV acceleration voltage, ×50 000 magnification) of the WS_2 chloroauric acid reaction products after centrifugation-based work-up and purification with SC (E, G) and SDS (F, H) as surfactant. In the case of decoration in SC, the stock dispersion consists of selectively edge decorated nanosheets isolated at high centrifugal accelerations (E) and nanosheets with significantly bigger nanoparticles on the basal plane isolated at low centrifugal acceleration (G). In the case of SDS, the stock dispersion consists of free gold nanoparticles (F) as well as ill-defined gold structures and non-edge decorated nanosheets that appear less electron transparent and therefore few-layered (H).

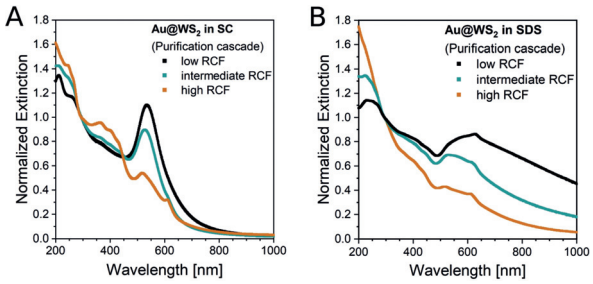

Figure 2. A),B) Normalized extinction spectra of WS_2 dispersions reacted with chloroauric acid with SC (A) and SDS (B) as surfactant after the purification cascade. In the case of SC, the spectrum of the dispersion isolated at high centrifugal acceleration is dominated by the excitonic transitions of WS_2, while the WS_2 signature cannot be clearly resolved in the SDS samples.

(Supporting Information, Chapter S3). In contrast, bulk WS_2 powder was found to react with $H[AuCl_4]$ in the absence of surfactant (Supporting Information, Figure S2). To gain further insights, a chloroauric acid concentration screening was performed and the amount of unreacted reagent (isolated in the supernatant after the high-speed centrifugation during the work-up) determined from extinction spectroscopy (Figure 3; Supporting Information, Figures S3–S5). The extinction spectra of the unreacted chloroauric acid for molar $H[AuCl_4]$:WS_2 ratios ranging from 0.1 to 8 equiv are displayed in Figure 3 A,B with SC (Figure 3 A) and SDS (Figure 3 B) as surfactant. The inset of the high energy region shows that no characteristic absorbance of $H[AuCl_4]$ is observed up to 4 equiv. The extinction coefficient of $H[AuCl_4]$ can be used to calculate the chloroauric acid concentration (see the Supporting Information) and hence the portion of reacted $H[AuCl_4]$. This is plotted for both SC and SDS as function of molar $H[AuCl_4]$:WS_2 ratio in Figure 3 C and D, respectively. Interestingly, the portion of reacted is close to unity up to 6 equiv in both cases, after which it drops, that is, not all $H[AuCl_4]$ is reduced. The saturation of chloroauric acid consumption at 6 equiv clearly points towards a stoichiometry that oxidizes both tungsten and sulfur to an oxidation state of +VI and therefore to their maximum oxidation state (Figure 3 E). The identity of the oxidized tungsten and sulfur compounds produced after complete oxidation is intentionally left blank (denoted as W(+VI) and S(+VI) in Figure 3 E), since their identity cannot be unambiguously assigned. To test this, we calculated the theoretical $H[AuCl_4]$ consumption based on this proposed reaction stoichiometry and included it in Figure 3 C,D. A remarkable agreement is observed with the exception of very low $H[AuCl_4]$ equiv (< 0.5 equiv) where the concentration of unreacted $H[AuCl_4]$ is overestimated. We attribute this to the presence of soluble reaction side products responsible to an onset of absorbance in the UV region without the characteristic $H[AuCl_4]$ peaks (inset in Figures 3 A, B). These could be for example water-soluble species like tungstates (WO_4^{2-}).

To confirm that the WS_2 is heavily oxidized, the reaction mixture without work-up or purification (SDS, 4 equiv $H[AuCl_4]$) was filtered, washed with water to remove water soluble species (such as residual surfactant and water-soluble

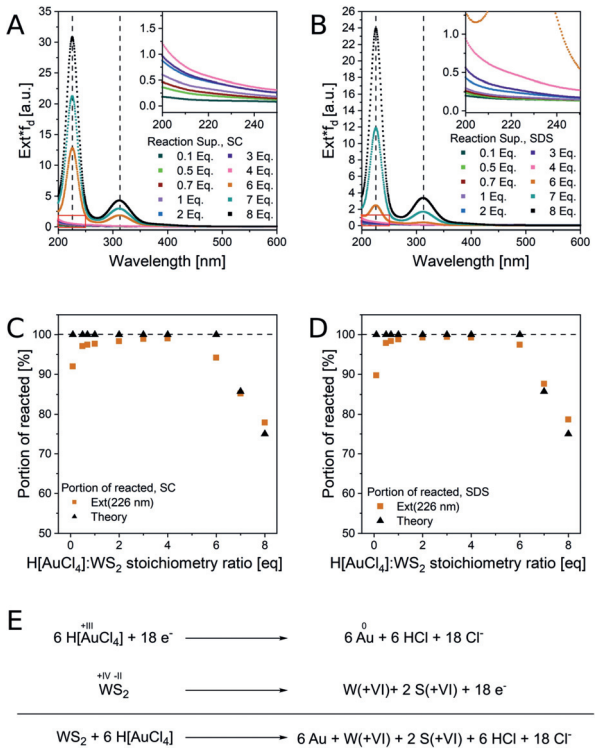

Figure 3. Extinction spectra multiplied with the dilution coefficient (f_d) of the acidified reaction supernatant removed during work-up for decoration in SC (A) and SDS (B). The insets show a magnification of the high energy region where the dominant absorbance of chloroauric acid is located. The characteristic peak is not observed for less than 4 equiv of $H[AuCl_4]$. Ext^*f_d is used to assess the extinction of the undiluted sample and therefore the total amount of chloroauric acid in the supernatant. Using the extinction coefficient $\varepsilon_{226\,nm}$, the portion of reacted was calculated from the extinction spectra and plotted versus the employed equiv of chloroauric acid (C, D). Black data points assume complete oxidation of WS_2 to the highest oxidation state of +VI for both W and S. E) The proposed redox reaction. The species W(+VI) and S(+VI) are left blank since the exact compounds produced cannot be assigned unambiguously.

oxidation products) and subjected to X-ray photoelectron spectroscopy (XPS). Note that in previous studies,[13] only purified samples were analyzed with XPS, which revealed no evidence of heavy oxidation of the WS_2. However, these could have simply been removed by the centrifugation-based purification. The Au 4f core level only show the $4f_{7/2}$ and $4f_{5/2}$ peaks at 84.0 and 87.7 eV, respectively (Supporting Information, Figure S6A). This indicates that only elemental gold and no unreacted chloroauric acid is present. This is also confirmed by the absence of signals that can be attributed to chlorine (Supporting Information, Figure S6C). In the sulfur core level spectrum, we see three sets of signals (Figure 4 A). Fitting the signals yields two doublets in the region between 160 and 166 eV assigned to $2p_{3/2}$ and $2p_{1/2}$ sulfur core levels, respectively, arising from two different sulfur species: sulfur bound to tungsten ($2p_{3/2}$ at 161.1 eV and $2p_{1/2}$ at 162.3 eV) and sulfur bound to gold ($2p_{3/2}$ at 162.4 eV and $2p_{1/2}$ at 163.6 eV). Furthermore, an intense doublet between 167 and 172 eV can be observed that is significantly shifted compared to the sulfur in oxidation state −II. Based on the high binding energy ($2p_{3/2}$

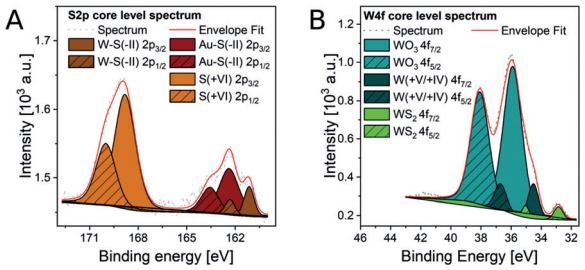

Figure 4. A),B) XPS analysis of WS_2 (in SDS) reacted with four equiv of chloroauric acid. The reaction mixture was filtered, washed with DI water, and the filter cake analyzed. A) S 2p and B) W 4f core-level spectra. The peaks were fitted using doublets with a fixed peak area ratio of 1:2 and 3:4 for p and d, respectively. Separation of the doublet spin–orbit components for W 4f was 2.17 eV and for S 2p 1.16 eV.

at 168.8 eV and $2p_{1/2}$ at 170.0 eV), it is assigned to sulfur in the oxidation state +VI, for example stemming from sulfates. These can either be produced during oxidation of WS_2 or indicate residual SDS surfactant. Owing to the intense washing of the sample and the high intensity of the signal, the latter seems unlikely as corroborated by the absence of sodium in the survey spectra (Supporting Information, Figure S6C). Similarly, we find the peaks of highest intensity in the tungsten core level spectrum (Figure 4B) at 36.0 and 38.1 eV, corresponding to $4f_{7/2}$ and $4f_{5/2}$ core level signals that we assign to tungsten trioxide or other W(+VI) species. In analogy, oxidized Mo(+VI) species were found after chloroauric acid treatment of chemically exfoliated MoS_2 and production of molybdic acid was suggested.[26] Further, we see two doublets with lower intensity at lower binding energies. The lowest binding energy doublet ($4f_{7/2}$ at 32.9 eV and $4f_{5/2}$ at 35.1 eV) corresponds to non-oxidized WS_2, which is a minor contribution to the overall signal. This demonstrates that, despite the removal of water-soluble oxidation products by filtration, the majority of WS_2 is heavily oxidized, but not completely decomposed. The doublet with $4f_{7/2}$ at 34.5 eV and $4f_{5/2}$ at 36.7 eV cannot be assigned unambiguously, but owing to its position it is likely an intermediate, not fully oxidized tungsten species. Similar assignments have been published previously for the CVD growth of WS_2 nanosheets from WO_3 precursors.[27]

XPS confirms the formation of tungsten(+VI) compounds as well as sulfur(+VI). Based on the above findings, we propose that the oxidation reaction itself is not selective towards edges or defects, but that $H[AuCl_4]$ is in principle capable of completely oxidizing LPE WS_2 to the highest oxidation state. In conjunction with the formerly reported[13] monolayer enrichment upon gold decoration, the monolayers appear more inert towards oxidation than few-layered materials. This is counterintuitive, since monolayers show the highest surface-to-volume ratio and are generally regarded as the most reactive. To rationalize this contradiction, we developed a simple model to explain the observed behavior of the system. The reaction mechanism hypothesized below also accounts for the different observations in the two surfactants in Figures 1 and 2.

An oxidant has multiple possible reaction pathways to attack a surfactant covered nanosheet suspended in an aqueous medium either on the exposed edges (green arrows, denoted as 1 in Figure 5) or the basal plane. The latter can occur either by reaction with exposed surface (purple arrows, denoted as 2 in Figure 5) or from in between the layers in the case of bi- and few-layer nanosheets if the reagent can intercalate between the sheets (blue arrow, denoted as 3 in Figure 5). We suggest that the facial amphiphile SC is densely packed on the surface thus blocking reaction pathway 2, resulting in an efficient shielding of the basal plane which slows down the reaction rate of this pathway. Hence, in monolayers, where the reaction pathway through intercalation cannot occur, oxidation of WS_2 mostly takes place at edges (Figure 5, left). With the linear amphiphile SDS, all reaction pathways can occur (Figure 5, right), albeit with different reaction rates as we will discuss further. Based on the findings shown below, we suggest that the reaction rate of pathway 2 is faster than pathway 1 and 3. As a result, an ill-defined mixture of gold structures and (partially) oxidized nanosheets is obtained with the degree of oxidation depending on the molar stoichiometry ratio of the reagents.

To verify that chloroauric acid is capable of penetrating the interlayer space, we conducted powder XRD on a sample of gold-decorated WS_2 to monitor changes to the crystal structure (Figure 6A). We chose a relatively low $H[AuCl_4]$:WS_2 stoichiometry ratio of 0.5 equiv to avoid complete disintegration of the WS_2. Importantly, all reflections characteristic for WS_2 are present with negligible shifts, albeit significantly broadened, as well as reflections that can be assigned to gold (fcc, green vertical lines in Figure 6A).[28] The relative peak intensities however change significantly. Some reflections apparently drop in intensity whereas others seem unusually enhanced in the chloroauric acid-treated WS_2 in comparison to the liquid-exfoliated reference. Generally, loss of intensity and peak broadening is expected upon exfoliation.[28a] For example, the reflections at 32.8° and 33.6° are barely visible in exfoliated WS_2. These peaks, present in WS_2 powder and absent in the exfoliated sample, are of higher intensity for the gold-decorated material. This could be attributed to formation of tungsten oxides, which are initially present in the unprocessed bulk material and are removed during exfoliation. Oxidation through chloroauric acid re-introduces these oxides. Peak broadening is also intensified in the decorated sample compared to the broadening upon

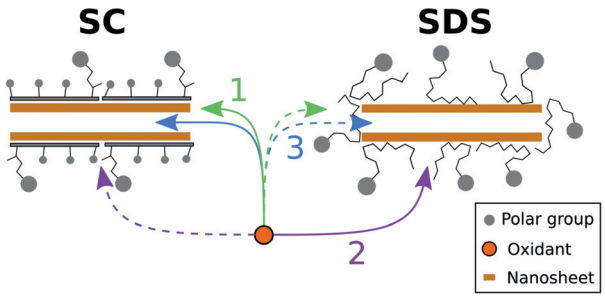

Figure 5. Proposed mechanism of the possible reaction pathways for a molecular oxidant at the nanosheet–solution interface. The dominant reaction pathway (solid lines) is determined by the surfactant coverage as well as the nanosheet layer number.

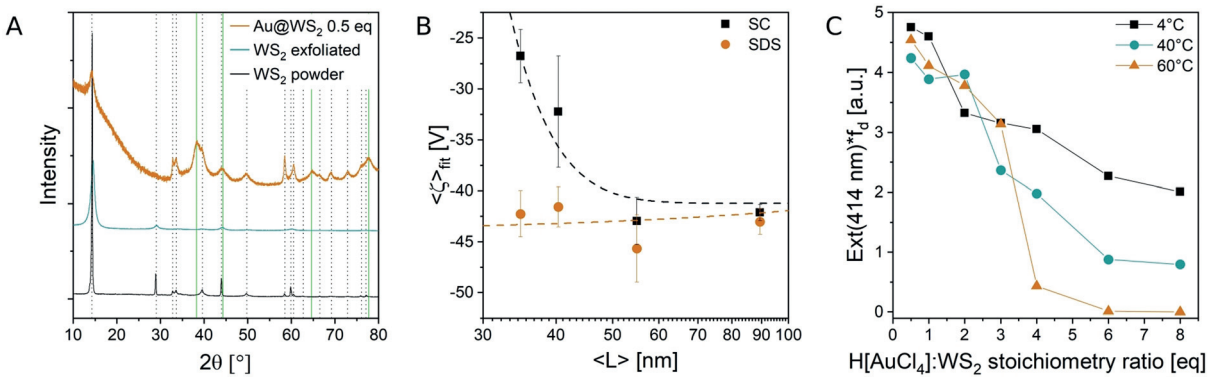

Figure 6. A) Powder XRD pattern of WS_2 powder before and after exfoliation as well as of a chloroauric acid treated sample (in SC, $H[AuCl_4]$:WS_2 stoichiometry ratio of 0.5 equiv). Black dotted lines correspond to signals found in pristine WS_2 powder, whereas the solid green lines indicate gold nanoparticle signals. Spectra are vertically offset for clarity. B) Zeta potentials of WS_2 dispersions in either SC or SDS surfactant solution with dotted lines as a guide for the eye. A significant size dependence is observed for SC, whereas barely any dependence is observed for SDS. This behavior is attributed to preferential adsoprtion of SC to the basal plane and non-preferential adsorption of SDS. C) Extinction at 414 nm multiplied with the dilution coefficient f_d of not size-selected, gold-decorated samples after work-up plotted as a function of chloroauric acid equiv at 4 °C, 40 °C, and 60 °C as a tool to monitor the amount of material in dispersion.

exfoliation, best seen at the (006) reflection at 44.0°. Also, a significant amount of non-Bragg scattering can be observed in the low angle region. Such a background can be present upon mechanical exfoliation due to the existence of single and few-layered particles.[28a] However, in this chloroauric acid-treated sample, the monolayer content is very low. Therefore, we attribute this background to degradation of the crystal lattice and decoupling of the nanosheets due to the growth of polydisperse gold nanoparticles in the interlayer space as a result of the intercalation of $H[AuCl_4]$. It should be noted that a contribution of the gold nanoparticles to the non-Bragg scattering background is also expected. Overall, the XRD analysis strongly suggests that intercalation of the chloroauric acid indeed takes place.

To gain experimental insights into the surfactant coverage of the WS_2 nanosheets, we conducted zeta potential measurements on samples of varying mean nanosheet length $\langle L \rangle$ (Figure 6B) produced from LPE and LCC (Supporting Information, Methods).[18b] Significant differences in behavior for SC and SDS are observed. For a fixed surfactant and WS_2 concentration, the zeta potential changes only slightly with decreasing nanosheet length for SDS, whereas a rapid decrease of zeta potentials can be observed for smaller nanosheets in SC. We attribute this behavior to the response of the surfactant coverage to the increasing edge-to-basal-plane ratio with decreasing $\langle L \rangle$. Furthermore, peak broadening can be seen in the zeta potential distributions for decreasing $\langle L \rangle$, more pronounced for SC (Supporting Information, Figure S7C). These findings are attributed to preferential adsorption of SC to the basal plane and thus a less optimal surfactant coverage for decreasing $\langle L \rangle$ and lower zeta potential magnitude. The peak broadening can be attributed to a more diffuse ion distribution at the shear plane. In contrast, SDS shows only a slight dependence on the nanosheet size and therefore should adsorb less specifically to the nanosheets. This can be readily rationalized from the chemical structure of the surfactants (Figure 1A,B): As a facial amphiphile and with its rigid structure, SC is more suitable for basal plane adsorption and adsorption at edges is less favorable, in contrast to the flexible structure of SDS.

These experiments confirm our proposed reaction in Figure 5. We note that we do not expect full shielding of the basal plane through the facial amphiphile SC. Instead, the likeliness of the oxidation to occur via different pathways depends on the relative reaction speed of each pathway and therefore on the kinetic barrier owing to the adsorbed surfactant. Hence, the relative contribution of the different reaction pathways to the total oxidation reaction is not only dependent on the type of surfactant, but also on adsorption/desorption kinetics. For example, it was shown in a NMR study, that a rapid exchange of bound and free SDS surfactant occurs on MoS_2 nanosheets, which are chemically very similar to the WS_2 nanosheets used herein.[20b]

The reaction speed of reaction pathway 2, that is, oxidation of the basal plane, should crucially depend on the surfactant coverage. In contrast to pathway 1 and 2, the intercalation-based pathway 3 is inaccessible for monolayer nanosheets and is therefore an explanation for the observed monolayer enrichment upon treatment with chloroauric acid. Basal plane oxidation (2) would probably lead to decomposition of the nanosheet, depending on the degree of oxidation defined by the molar stoichiometry ratio of the reagents. Since the oxidation at the edges (1) has probably the lowest kinetic barrier (in the case of SC) as well as benefits from the formation of thermodynamically favored sulfur–gold bonds,[13] it should proceed the fastest resulting in the nucleation of nanoparticles at edges. When performed in SDS, with its flexible structure, no selective nanoparticle edge decoration is observed, which suggests that edge sites are partially blocked which also imposes a kinetic barrier for intercalation. The discarded material in the work-up sediment consists of large gold aggregates and undecorated nanosheets that appear very thick (Figure 1E, G), which confirms this.[22] Note that free Au nanoparticles are efficiently solubilized and stabilized by SDS, but not SC. This leads the basal plane oxidation pathway (2) as the dominant oxidation taking place

in SDS, leading to degradation of the nanosheets. In contrast, in SC, oxidation occurs dominantly at edges and via intercalation due to basal plane shielding.

To test our model further, we examined the reaction performed in presence of SC at different temperatures. Higher temperatures are expected to accelerate the surfactant adsorption/desorption kinetics, resulting in temporarily bare surface and hence an increase in reaction speed for pathway 2 (for a discussion, see the Supporting Information). To test this, we performed the concentration screening at 4 °C, 40 °C, and 60 °C and evaluated the reaction products using extinction spectroscopy as described above. Under identical work up conditions, less WS_2-based material can be collected for comparable chloroauric acid concentrations in the sample after work up as well as in the separated sediment for increasing temperatures (Supporting Information, Figures S8, S9). This can readily be seen by monitoring the product of extinction at 414 nm (signal stemming mostly from WS_2) and dilution coefficient f_d, which reflects the amount of material in dispersion. $Ext^{*}f_d$ is decreasing in all cases with increasing chloroauric acid:WS_2 stoichiometry ratio, but faster at higher temperatures (Figure 6C). This indicates that the increasing temperatures lead to increased production of water-soluble oxidation products owing to desorption of SC from the nanosheets. The spectral shape of WS_2 also deteriorates more quickly for higher temperatures when using higher chloroauric acid equiv, further showing the increasing oxidation of WS_2 (Supporting Information, Figures S8, S9) at elevated temperatures.

Conclusion

In this work, we demonstrated the importance of the choice of surfactant and its impact on the reactivity of dispersed nanosheets. Decorating WS_2 nanosheets with gold nanoparticles utilizing chloroauric acid shows very different reaction products in aqueous solutions with a facial and a linear amphiphile as surfactant. The oxidation reaction itself was shown to be not specific to defects in WS_2, and the formerly reported monolayer enrichment[13] is rather related to reaction control imposed by the surfactant coverage. Hence, in contrast to graphite,[29] the site-selective oxidation of WS_2 does not seem to be intrinsic to the material.

Hence, we propose a simple model in which the employed surfactant governs the dominant reaction pathway through suppression of competing reaction channels, depending on the adsorption preferences of the surfactant. We further performed size-dependent zeta potential measurements to investigate the surfactant nanosheet interaction. Additionally, a series of decoration reactions at different temperatures was performed and deterioration of the reaction products upon increase in temperature was observed, which is probably due to surfactant desorption kinetics. With this work, we want to stress the importance of choosing a suitable surfactant for the targeted functionalization since it can have a significant impact on the possible reaction pathways at the nanosheet solution interface and ultimately on the functionalization product. Control over the surfactant coverage has a great potential to enable selective functionalization of low dimensional materials without altering the functionalization reagents and can therefore serve as a potent tool in tailoring the properties of materials.

Acknowledgements

We acknowledge the European Union under grant agreement no. 881603 Graphene Flagship-core 3. C.B. acknowledges support from the German research foundation (DFG) under grant agreement Emmy-Noether, BA4856/2-1. We thank the Electron Microscopy Core Facility (EMCF) at the European Molecular Biology Laboratory (EMBL) for their support.

Conflict of interest

The authors declare no conflict of interest.

Keywords: functionalization · layered compounds · nanostructures · surfactants · transition-metal dichalcogenides

[1] K. S. Novoselov, A. Mishchenko, A. Carvalho, A. H. Castro Neto, *Science* **2016**, *353*, aac9439.
[2] M. Chhowalla, H. S. Shin, G. Eda, L.-J. Li, K. P. Loh, H. Zhang, *Nat. Chem.* **2013**, *5*, 263 – 275.
[3] V. Nicolosi, M. Chhowalla, M. G. Kanatzidis, M. S. Strano, J. N. Coleman, *Science* **2013**, *340*, 1226419.
[4] J. N. Coleman, *Acc. Chem. Res.* **2013**, *46*, 14 – 22.
[5] J. Kang, V. K. Sangwan, J. D. Wood, M. C. Hersam, *Acc. Chem. Res.* **2017**, *50*, 943 – 951.
[6] a) S. Bertolazzi, M. Gobbi, Y. Zhao, C. Backes, P. Samorì, *Chem. Soc. Rev.* **2018**, *47*, 6845 – 6888; b) S. Eigler, A. Hirsch, *Angew. Chem. Int. Ed.* **2014**, *53*, 7720 – 7738; *Angew. Chem.* **2014**, *126*, 7852 – 7872; c) A. Hirsch, F. Hauke, *Angew. Chem. Int. Ed.* **2018**, *57*, 4338 – 4354; *Angew. Chem.* **2018**, *130*, 4421 – 4437; d) A. Stergiou, N. Tagmatarchis, *Chem. Eur. J.* **2018**, *24*, 18246 – 18257.
[7] a) D. Voiry, A. Goswami, R. Kappera, C. de Carvalho Castro e Silva, D. Kaplan, T. Fujita, M. Chen, T. Asefa, M. Chhowalla, *Nat. Chem.* **2015**, *7*, 45 – 49; b) K. C. Knirsch, N. C. Berner, H. C. Nerl, C. S. Cucinotta, Z. Gholamvand, N. McEvoy, Z. Wang, I. Abramovic, P. Vecera, M. Halik, S. Sanvito, G. S. Duesberg, V. Nicolosi, F. Hauke, A. Hirsch, J. N. Coleman, C. Backes, *ACS Nano* **2015**, *9*, 6018 – 6030.
[8] a) S. S. Chou, M. De, J. Kim, S. Byun, C. Dykstra, J. Yu, J. Huang, V. P. Dravid, *J. Am. Chem. Soc.* **2013**, *135*, 4584 – 4587; b) A. Hirsch, X. Chen, P. Denninger, T. Stimpel-Lindner, E. Spiecker, G. S. Duesberg, C. Backes, K. C. Knirsch, *Chem. Eur. J.* **2020**, *26*, 6535 – 6544; c) A. Förster, S. Gemming, G. Seifert, D. Tománek, *ACS Nano* **2017**, *11*, 9989 – 9996.
[9] C. Backes, N. C. Berner, X. Chen, P. Lafargue, P. LaPlace, M. Freeley, G. S. Duesberg, J. N. Coleman, A. R. McDonald, *Angew. Chem. Int. Ed.* **2015**, *54*, 2638 – 2642; *Angew. Chem.* **2015**, *127*, 2676 – 2680.
[10] X. S. Chu, A. Yousaf, D. O. Li, A. A. Tang, A. Debnath, D. Ma, A. A. Green, E. J. G. Santos, Q. H. Wang, *Chem. Mater.* **2018**, *30*, 2112 – 2128.
[11] M. Vera-Hidalgo, E. Giovanelli, C. Navío, E. M. Pérez, *J. Am. Chem. Soc.* **2019**, *141*, 3767 – 3771.
[12] a) R. Canton-Vitoria, H. B. Gobeze, V. M. Blas-Ferrando, J. Ortiz, Y. Jang, F. Fernández-Lázaro, Á. Sastre-Santos, Y. Nakanishi, H. Shinohara, F. D'Souza, N. Tagmatarchis, *Angew.*

Chem. Int. Ed. **2019**, *58*, 5712 – 5717; *Angew. Chem.* **2019**, *131*, 5768 – 5773; b) R. Canton-Vitoria, Y. Sayed-Ahmad-Baraza, M. Pelaez-Fernandez, R. Arenal, C. Bittencourt, C. P. Ewels, N. Tagmatarchis, *NPJ 2D Mater. Appl.* **2017**, *1*, 13.

[13] J. R. Dunklin, P. Lafargue, T. M. Higgins, G. T. Forcherio, M. Benamara, N. McEvoy, D. K. Roper, J. N. Coleman, Y. Vaynzof, C. Backes, *NPJ 2D Mater. Appl.* **2018**, *1*, 43.

[14] a) M. F. Islam, E. Rojas, D. M. Bergey, A. T. Johnson, A. G. Yodh, *Nano Lett.* **2003**, *3*, 269 – 273; b) R. M. F. Fernandes, B. Abreu, B. Claro, M. Buzaglo, O. Regev, I. Furó, E. F. Marques, *Langmuir* **2015**, *31*, 10955 – 10965.

[15] a) M. Lotya, P. J. King, U. Khan, S. De, J. N. Coleman, *ACS Nano* **2010**, *4*, 3155 – 3162; b) S. Wang, M. Yi, Z. Shen, *RSC Adv.* **2016**, *6*, 56705 – 56710.

[16] A. Griffin, A. Harvey, B. Cunningham, D. Scullion, T. Tian, C.-J. Shih, M. Gruening, J. F. Donegan, E. J. G. Santos, C. Backes, J. N. Coleman, *Chem. Mater.* **2018**, *30*, 1998 – 2005.

[17] A. Griffin, K. Nisi, J. Pepper, A. Harvey, B. Szydłowska, J. N. Coleman, C. Backes, *Chem. Mater.* **2020**, *32*, 2852 – 2862.

[18] a) P. Ramalingam, S. T. Pusuluri, S. Periasamy, R. Veerabahu, J. Kulandaivel, *RSC Adv.* **2013**, *3*, 2369 – 2378; b) C. Backes, B. M. Szydłowska, A. Harvey, S. Yuan, V. Vega-Mayoral, B. R. Davies, P.-l. Zhao, D. Hanlon, E. J. G. Santos, M. I. Katsnelson, W. J. Blau, C. Gadermaier, J. N. Coleman, *ACS Nano* **2016**, *10*, 1589 – 1601; c) M. S. Arnold, J. Suntivich, S. I. Stupp, M. C. Hersam, *ACS Nano* **2008**, *2*, 2291 – 2300.

[19] S. Lin, C.-J. Shih, M. S. Strano, D. Blankschtein, *J. Am. Chem. Soc.* **2011**, *133*, 12810 – 12823.

[20] a) N. R. Tummala, A. Striolo, *J. Phys. Chem. B* **2008**, *112*, 1987 – 2000; b) A. Gupta, V. Arunachalam, S. Vasudevan, *J. Phys. Chem. Lett.* **2015**, *6*, 739 – 744; c) A. Gupta, S. Vasudevan, *J. Phys. Chem. C* **2018**, *122*, 19243 – 19250.

[21] L. B. Pártay, P. Jedlovszky, M. Sega, *J. Phys. Chem. B* **2007**, *111*, 9886 – 9896.

[22] M. Faraday, *Philos. Trans. R. Soc. London* **1857**, *147*, 145 – 181.

[23] S. P. Ogilvie, M. J. Large, M. A. O'Mara, P. J. Lynch, C. L. Lee, A. A. K. King, C. Backes, A. B. Dalton, *2D Mater.* **2019**, *6*, 031002.

[24] G. T. Forcherio, J. R. Dunklin, C. Backes, Y. Vaynzof, M. Benamara, D. K. Roper, *AIP Adv.* **2017**, *7*, 075103.

[25] J. A. Wilson, A. D. Yoffe, *Adv. Phys.* **1969**, *18*, 193 – 335.

[26] J. Kim, S. Byun, A. J. Smith, J. Yu, J. Huang, *J. Phys. Chem. Lett.* **2013**, *4*, 1227 – 1232.

[27] K. M. McCreary, A. T. Hanbicki, G. G. Jernigan, J. C. Culbertson, B. T. Jonker, *Sci. Rep.* **2016**, *6*, 19159.

[28] a) J. Djamil, A.-L. Hansen, C. Backes, W. Bensch, U. Schürmann, L. Kienle, A. Düvel, P. Heitjans, *Nanoscale* **2018**, *10*, 21142 – 21150; b) S. Pyrpassopoulos, D. Niarchos, G. Nounesis, N. Boukos, I. Zafiropoulou, V. Tzitzios, *Nanotechnology* **2007**, *18*, 485604.

[29] S. Seiler, C. E. Halbig, F. Grote, P. Rietsch, F. Börrnert, U. Kaiser, B. Meyer, S. Eigler, *Nat. Commun.* **2018**, *9*, 836.

Manuscript received: April 23, 2020
Accepted manuscript online: May 25, 2020
Version of record online: June 25, 2020

